Slow Variability in the Equatorial West-Central Pacific in Relation to ENSO

R. H. WEISBERG AND C. WANG

Department of Marine Science, University of South Florida, St. Petersburg, Florida

(Manuscript received 23 April 1996, in final form 20 August 1996)

ABSTRACT

Six years of upper-ocean velocity, temperature, and surface wind data collected in the west-central Pacific at 0°, 170°W reveal a slow ocean dynamical mode associated with the El Niño–Southern Oscillation (ENSO). Latent and sensible heat flux calculations using the basin-wide Tropical Atmosphere Ocean (TAO) array data show a coincident, slow ocean–atmosphere thermodynamical mode. Beginning with the La Niña conditions in 1988 through the peak El Niño conditions in 1992 the Equatorial Undercurrent (EUC) speed decreased along with the surface zonal wind stress and the zonal pressure gradient. Simultaneous with these were increasing trends in the Richardson number above the EUC core and in sea surface temperature (SST). After peak warming was achieved, the variations in all of these quantities reversed in a movement toward their previous La Niña conditions. As this evolved within the ocean the sensible and latent heat fluxes increased with large values emanating eastward from the western Pacific. The largest interannual perturbations, then, for both the surface momentum and heat flux quantities during this recent ENSO cycle were within the west-central Pacific, the transition region between the warmest waters found in the western Pacific warm pool and the coldest waters found in the eastern Pacific cold tongue. The observed ocean and atmosphere variability represents a positive feedback. This raises a question about the origin of negative feedback that is necessary for the coupled system to oscillate. Arguing from the standpoint of a Gill atmosphere and observed SST–sea level pressure correlation patterns, the paper draws a connection between condensation heating in the equatorial west-central Pacific and easterly winds over the equatorial western Pacific during the mature phase of El Niño. The formation of such easterlies by ocean–atmosphere coupling over the western Pacific is hypothesized as providing a negative feedback for reversing the sign of anomalous SST in the equatorial central Pacific. This mechanism may complement, but it is different from, the delayed oscillator mechanism for ENSO.

1. Introduction

The equatorial west-central Pacific, separating the western Pacific warm pool from the eastern Pacific cold tongue, is characterized by large interannual surface wind stress variability, and it is the region through which the air–sea interactions associated with the El Niño–Southern Oscillation (ENSO) evolve. Recognizing a data void along the equator within this vast, transitional region, measurements of upper-ocean velocity, temperature, and surface winds were initiated at 0°, 170°W in May 1988 as part of the Tropical Atmosphere Ocean (TAO) array designed to monitor the air–sea interactions that comprise ENSO. In collaboration with (the late) Stanley B. Hayes a subsurface moored acoustic Doppler current profiler (ADCP) was deployed for upper-ocean velocity along with an ATLAS mooring for upper-ocean temperature and surface winds. These measurements continue to date.

The phenomenology of ENSO is the subject of several reviews (e.g., Philander 1990; Diaz and Markgraf 1992; Neelin et al. 1994). It consists of a warm phase (El Niño) and a cold phase (La Niña) with this cycle occurring roughly twice per decade. Conceptual ideas have been promoted to explain the oscillations that are intrinsic to models of the coupled ocean–atmosphere system. Of these, the slow-mode (e.g., Hirst 1986, 1988) and the delayed oscillator (e.g., Suarez and Schopf 1988; Battisti and Hirst 1989) paradigms provide candidate mechanisms. However, a quantitative understanding of ENSO remains elusive, as evidenced by the protracted nature of the most recent warm phase.

The west-central Pacific measurements presented herein began at the peak of the previous La Niña. Weisberg and Hayes (1995) describe the initial 3 yr of data, concentrating on annual, intraseasonal, and higher frequency variability. A developing interannual trend was evident, but the dataset was too short to pursue this. Additional years of data now available suggest a slow mode of ENSO wherein observations of SST variability in the west-central equatorial Pacific are hypothesized as arising from a fully three-dimensional, ocean circulation dynamical mode, feeding back positively with the overlying surface winds. A corollary ocean–atmosphere thermodynamical mode is further suggested by the

Corresponding author address: Dr. Robert H. Weisberg, Department of Marine Science, University of South Florida, 140 Seventh Avenue South, St. Petersburg, FL 33701-5016.
E-mail: weisberg@marine.usf.edu

evolving fields of the sensible and latent heat fluxes and their (Bowen) ratio. In both the ocean and atmosphere, these coupled modes may be described as slow divergence modes whose nature can be characterized by SST and air temperature (AT) variability that is governed by boundary layer divergences. With the ocean dynamical part of the slow mode being a positive feedback leading to anomaly growth, a negative feedback enabling the coupled system to oscillate must occur by other means. This is hypothesized as an atmospheric dynamical response to west-central Pacific thermodynamic forcing that ultimately results in easterly winds over the western part of the basin that provide a negative feedback. The hypothesis, thus conceived, is a hybrid between the slow-mode and delayed oscillator paradigms with 1) the west-central and western portions of the basin being important regions for ENSO, and 2) with free equatorial waves reflecting at the western boundary being supplanted by a forced wave response that originates in the western Pacific.

The paper is organized as follows: section 2 describes the data and the evidence supporting slow, interannual ocean dynamical variability. Section 3 provides further analyses and evidence supporting slow, interannual ocean–atmosphere thermodynamic variability. Higher-frequency variations in SST relative to the ocean dynamics and ocean–atmosphere interaction thermodynamics are also developed for the purpose of elucidating the nature of the processes that impact intraseasonal versus interannual variations. Section 4 summarizes the results and develops the hypothesis advanced.

2. The data

Data on the ocean dynamical mode of variability derive primarily from the combined subsurface ADCP and surface ATLAS moorings deployed at 0°, 170°W for which the instrumentation and processing procedures are described in Weisberg and Hayes (1995). SST, subsurface temperature, surface wind, and AT data from other sites of the TAO array have also been used to estimate the zonal gradients in SST and pressure at 0°, 170°W and to estimate the latent and sensible heat fluxes across the equatorial Pacific Ocean. To examine the role of horizontal advection on SST, the higher-resolution Reynolds' blended SST product (Reynolds and Smith 1995) has been used to estimate the zonal and meridional SST gradients.

The subsurface data extend from May 1988 to March 1994, generally between depths of 30–290 m, with small variations due to different annual deployments. Contours of the 10-day low-pass filtered zonal (u) and meridional (v) velocity components and temperature (T) are shown as a function of depth and time in Figs. 1a, 1b, and 1c, respectively. In general, the core speed of the Equatorial Undercurrent (EUC) shows a decreasing trend during this time interval. At the beginning of the record, the core speed was greater than 80 cm s^{-1} and reached 125 cm s^{-1} in June 1988. Near the end of the record the core speed was only about 50 cm s^{-1}. As will be shown, similar decreasing trends existed in both the zonal pressure gradient (ZPG) at the EUC core and the surface easterly wind stress (τ^x). Along with this interannual trend there is an annual cycle in the depth of the EUC core with the highest speeds found deeper in (boreal) winter and shallower in summer. At this location the deepest core depth was about 220 m, the shallowest about 90 m with the average being about 160 m. Either drawing a line through the shallowest core depths achieved in summer or fitting a linear least-squares trend shows that the EUC core deepened from the beginning to the end of the record by about 30 m.

An annual cycle is also observed in the surface South Equatorial Current (SEC). During winter, the SEC tends to be well developed and it penetrates deeply with the mixed layer. During spring and summer, as the EUC shoals, the surface flow may reverse to be eastward, contiguous with the EUC. Superimposed upon this annual cycle are large, higher-frequency variations that are most prominent in the SEC during winter. These intraseasonal oscillations in the near-surface zonal currents are associated with Kelvin waves propagating from the west (e.g., Knox and Halpern 1982; McPhaden and Taft 1988; Kessler and McPhaden 1995) and modified by forcing along the way. Beginning in November 1991, with the onset of the protracted El Niño, there is a particularly pronounced set of such reversing surface jets with surface eastward speed exceeding 120 cm s^{-1} while the EUC core speed is only around 40 cm s^{-1}. Despite continued El Niño conditions, these jets are not as pronounced during 1993 and they are absent during 1994. Another interesting result is layers of westward flow located between eastward flow above and below in December 1991, January 1992, and March 1992. Although Hisard et al. (1970) and McPhaden et al. (1990) observed similar behavior farther west at 0°, 170°E and 0°, 165°E, respectively, this layered flow regime at 0°, 170°W is unique to the protracted ENSO warm event.

In contrast to u, v oscillates at relatively higher frequency. In particular, during fall 1988 and winter 1989, a set of regular, 3-week period oscillations associated with tropical instability waves are observed (Weisberg and Hayes 1995). This is the only year of record, thus far, that shows a prominent instability wave season in the west-central Pacific. A subtle interannual variation is also apparent. From September 1989 to April 1990 and again from March 1991 to December 1991, upon averaging out the higher frequencies, the direction of the meridional flow on the equator is preferentially northward, unlike other times when it is nearly zero. This may have bearing upon the hemispheric origin and temperature of water being upwelled near the equator. Similar observations are described by Qiao and Weisberg (1997) for currents centered about 0°, 140°W from May 1990 to June 1991. The mean flows south were

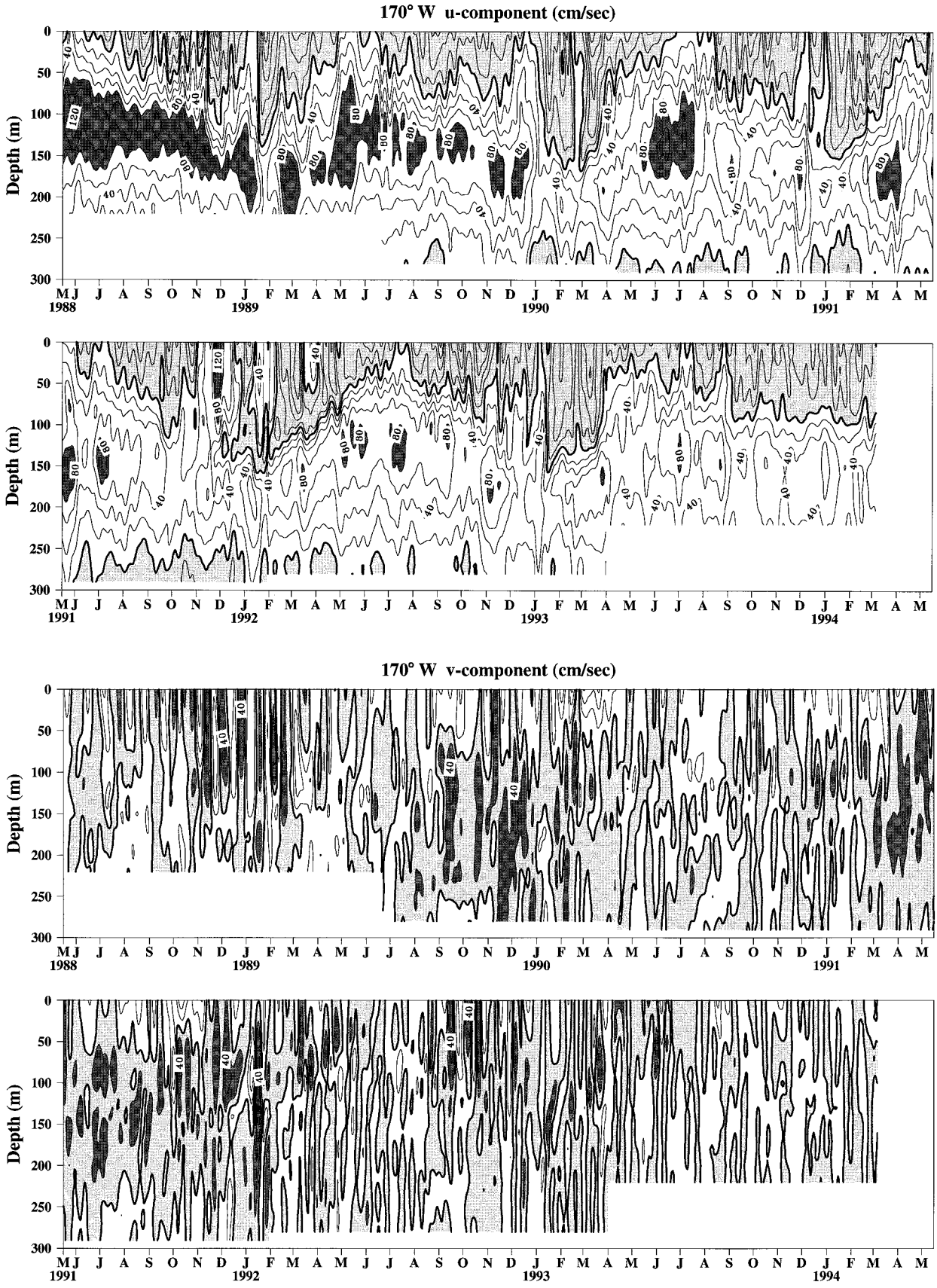
170° W u-component (cm/sec)
Depth (m)
0
50
100
150
200
250
300
M J J A S O N D J F M A M J J A S O N D J F M A M J J A S O N D J F M A M
1988
1989
1990
1991
1991
1992
1993
1994
170° W v-component (cm/sec)
Depth (m)
M J J A S O N D J F M A M J J A S O N D J F M A M J J A S O N D J F M A M
1988
1989
1990
1991
1991
1992
1993
1994

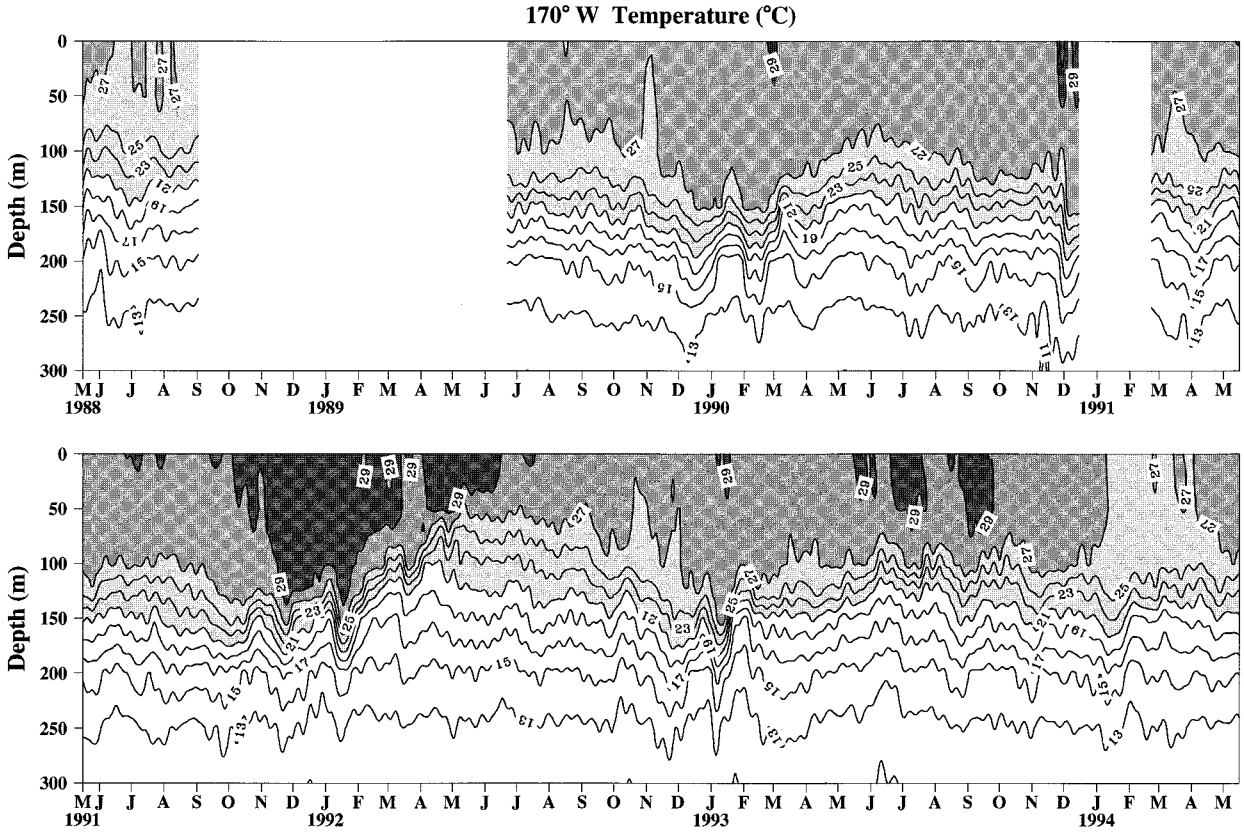

FIG. 1c. Temperature as a function of time and depth at 0°, 170°W from May 1988 through March 1994, low-pass filtered to remove oscillations on timescales shorter than 10 days. The surface measurement is at 1-m depth and the vertical resolution is 25 m from the surface to 150-m depth and then 50–300-m depth. The contour interval is 2°C, with stippling denoting temperatures in excess of 21°C.

stronger than those north of the equator, but the divergence was still centered on the equator.

Most noticeable in the isotherms are annual and intraseasonal variations. The thermocline, as characterized by the 20°C isotherm, is shallower in summer and deeper in winter, and intraseasonal variations are observed each winter (least so in 1994). The interannual variations are more subtle. For the protracted El Niño, the warmest waters (greater than 29°C) during 1991–92 last about one-half year beginning late in 1991 with a second weaker warming occurring the following year. During the initial 1991–92 warming the thermocline depth varies from deep to shallow in contrast with the secondary warming where the thermocline depth is relatively steady. Thus, interannual variations in thermocline depth at 0°, 170°W are not well correlated with SST.

The vertical distributions of the record-length means for these quantities are shown in Fig. 2 along with the estimated $\tan^{-1}$ (Ri). Here, Ri, the Richardson number, defined as the buoyancy frequency squared divided by the velocity shear squared, is computed as $\mathrm{Ri} = (\alpha g \partial T/\partial z)/[(\partial u/\partial z)^2 + (\partial v/\partial z)^2]$, where $\alpha = 8.75 \times 10^{-6}\ (T + 9)\ ^\circ\mathrm{C}^{-1}$ (Hayes et al. 1991) is the thermal expansion coefficient. It is noted that $\tan^{-1}(\mathrm{Ri})$ is approximately equal to Ri for small Ri. With the EUC core collocated with the thermocline, the velocity shears are largest and the temperature gradient is smallest above and below the core. Therefore, Ri has a minimum above the core, a maximum at the core, and a secondary minimum below the core. This suggests that vertical mixing is most intense above the EUC core (e.g., Peters et al. 1988).

As a continuous feature over nearly the entire width

←

FIG. 1. (a) The u component of velocity as a function of time and depth at 0°, 170°W from May 1988 through March 1994 low-pass filtered to remove oscillations on timescales shorter than 10 days. The vertical resolution is 10 m between the deepest level shown and 30 m. The values from 20 m to the surface are estimated by extrapolating the vertical shear between 40 and 30 m. Lightly stippled regions denote westward flow highlighting the surface SEC. Clear regions denote the eastward flowing EUC with darkly stippled regions denoting eastward flows in excess of 80 cm s^{-1} at the EUC core. (b) The v component of velocity as a function of time and depth at 0°, 170°W from May 1988 through March 1994 low-pass filtered to remove oscillations on timescales shorter than 10 days. The vertical resolution is 10 m between the deepest level shown and 30 m. The values from 20 m to the surface are estimated by extrapolating the vertical shear between 40 and 30 m. Stippled regions denote northward flow with dark stippling in excess of 40 cm s^{-1}. Clear regions denote southward flow.

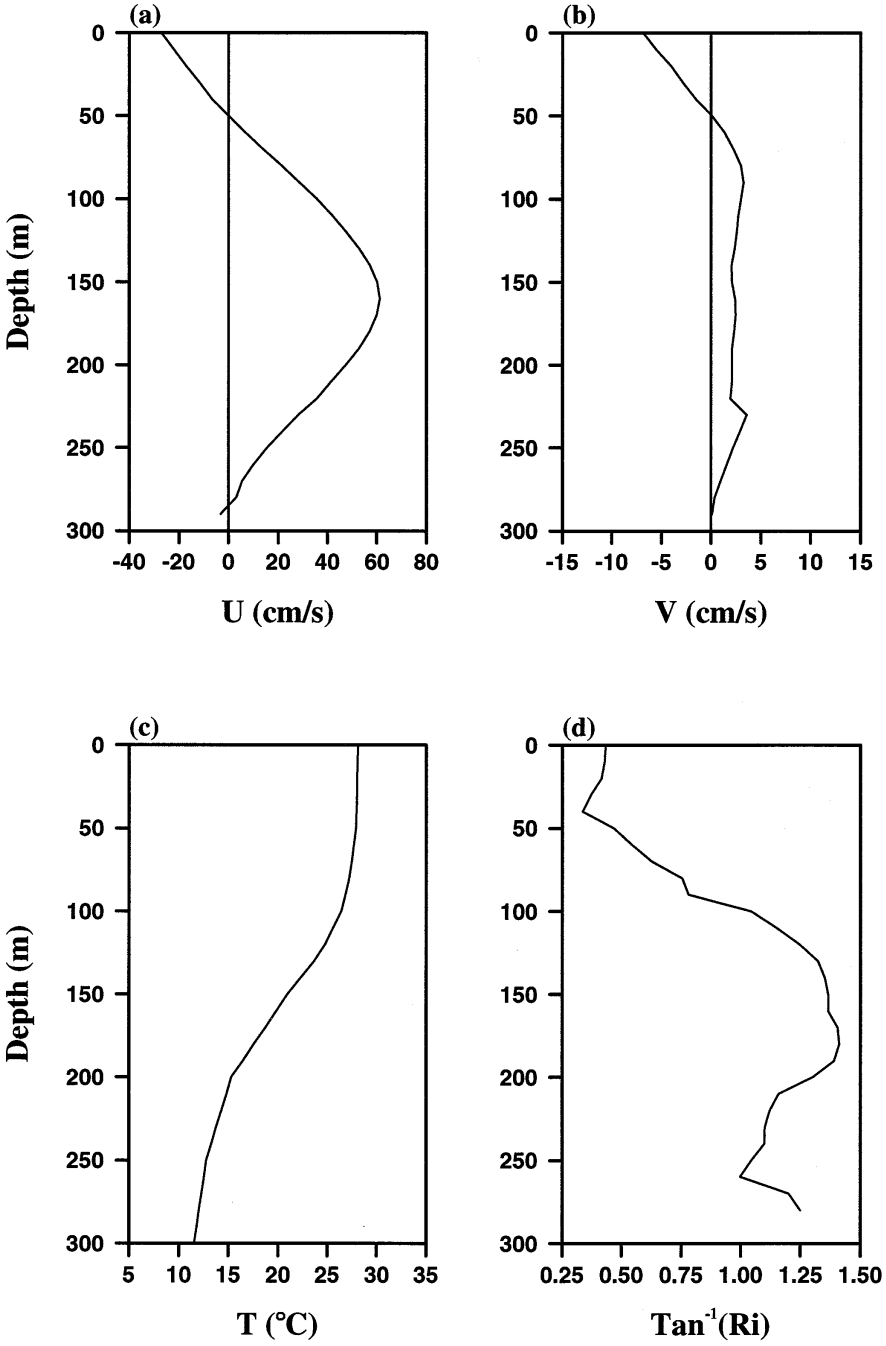

FIG. 2. Record-length mean vertical distributions for (a) the u component of velocity, (b) the v component of velocity, (c) temperature, and (d) Tan^{-1} (Ri).

of the Pacific Ocean, the speed of the EUC increases across the central Pacific from relatively small values in the west to relatively large values in the east. To this zonal variation in EUC core speed, evidence has now been presented of an interannual trend. Upon filtering out oscillations on timescales shorter than 30 days, Fig. 3a shows the EUC core speed, core depth, and the ZPG estimated at the core depth; Fig. 3b shows SST and τ^x and Fig. 3c shows the $\tan^{-1}$(Ri) averaged over the mixed layer (defined here as the layer, generally 50–100 m deep, below which temperature decreases by 0.5°C from its value at 1 m). The EUC core speed and depth vary annually with the speed tending to be largest when the core is shallowest in summer, and conversely in winter. Superimposed upon this (along with intraseasonal variability) is the interannual trend, most noticeable from

the 1988 La Niña conditions to the peak winter 1992 El Niño conditions. The ZPG at the core depth shows a similar trend, and as the core speed and ZPG decrease, the core depth slowly deepens. With the upper-ocean shear related to the core speed, as the core speed decreases there is a concomittant increase in Ri from values less than 0.25 at the beginning of the record to values greater than 0.25 thereafter. Along with these ocean dynamical variables is a secular rise in SST and a secular decrease in τ^x.

3. Analyses

a. Vertically integrated zonal momentum balance

The terms that can be estimated (Fig. 4) include the local acceleration ($\partial u/\partial t$), the local $\tau^x = \rho_a C_D \sqrt{u_a^2 + v_a^2}\, u_a$ (with drag coefficient $C_D = 1.43 \times 10^{-3}$ and air density $\rho_a = 1.225$ kg m^{-3}), and the ZPG (by centered difference between 0°, 140°W and 0°, 165°E). On interannual timescales, τ^x and the integrated ZPG covary with similar secular decreases from maximum values during the 1988 La Niña to minimum values during the winter 1992 peak El Niño. While both time series then increase, following the winter 1992 period of westerly winds and wind bursts, their magnitudes remain lower than their previous La Niña values. On intraseasonal timescales, covariation is observed in all three time series. In particular, the westerly wind burst events during the October 1991 to April 1992 period are associated with sign reversals of the integrated ZPG, with the ZPG lagging τ^x by about one month. This implies that the ZPG is responding to τ^x. In constrast to the integrated ZPG, the integrated $\partial u/\partial t$ oscillates with much larger amplitude. This frequency mismatch between the integrated ZPG and $\partial u/\partial t$ suggests that the TAO array does not resolve the spatial structure of the intraseasonal and higher frequency oscillations. Resolving the ZPG for these higher frequencies requires a closer spacing between TAO moorings.

The covariability among these three time series is explored using ordinary and multiple coherence analyses as shown in Fig. 5. If τ^x and the integrated ZPG balance, as appears to be the case at interannual timescales, then an integrated $\partial u/\partial t$ is not necessary. If such balance does not obtain, as expected for timescales shorter than annual (since it takes approximately 1 yr for a Kelvin wave and its first mode Rossby wave reflection to transit the basin), then an integrated $\partial u/\partial t$ is necessary as the residual between τ^x and the integrated ZPG. The ordinary coherence between τ^x and the integrated ZPG shows prominent bands of coherence at interannual and intraseasonal timescales. At interannual timescales the phase is zero and the transfer function amplitude (not shown) is unity, implying that these two terms balance. At intraseasonal timescales the phase is positive with the ZPG lagging τ^x, so these two terms do not balance. The multiple coherence between τ^x and the integrated ZPG with the integrated $\partial u/\partial t$ is high over intraseasonal timescales and the partial coherences, either excluding the ZPG or τ^x, shows that both of these time series are of equal importance in determining the vertically integrated $\partial u/\partial t$. Thus, at interannual timescales, τ^x and the integrated ZPG tend to balance, while at intraseasonal timescales the imbalance between these gives rise to a vertically integrated $\partial u/\partial t$ as postulated.

The in-phase covariability at interannual timescales between τ^x and the integrated ZPG is particularly relevant to ENSO. Physically, the density and zonal pressure gradients associated with the east–west thermocline slope are supported by τ^x. As τ^x decreases, so will the ZPG, and if this causes an increase in SST through ocean dynamics then τ^x will decrease further resulting in a positive ocean–atmosphere feedback leading to mature phases of ENSO.

b. The ZPG in relation to the EUC

The ZPG, as the driving force for the EUC, must play a primary role in maintaining the EUC. Figure 3a shows that the EUC core speed tends to be small when the core is deep in winter and during the warm phase of ENSO, and conversely in summer and during the cold phase of ENSO and that the slow, interannual variations in the core speed, core depth, and ZPG at the core occur in phase. These interannual variations are consistent with the ENSO evolution from the 1988 La Niña conditions through the protracted 1991–94 El Niño conditions. During this time the ocean–atmosphere system associated with the western Pacific warm pool region sidled eastward, resulting in reduced τ^x, ZPG, and a deepened EUC and thermocline over the west-central Pacific.

A coherence analysis between the EUC core speed and the ZPG at the core (Fig. 6) confirms the in-phase covariability. If we hypothesize a linear momentum balance between the ZPG and the vertical stress divergence at the core—that is, $(1/\rho)\partial p/\partial x = A\partial^2 u/\partial z^2$, then we can estimate a vertical eddy viscosity coefficient (from the transfer function amplitude) that would be necessary to balance the ZPG. Such eddy viscosity would have to be order 10^{-3} m^2 s^{-1}, which is unrealistically large (e.g., Peters et al. 1988; Lien et al. 1995), suggesting that we reject this hypothesis. Moreover, the in-phase relationship between the ZPG and the EUC core speed implies nonlinearity, because a local acceleration would give rise to a quadrature relationship. This implied nonlinear momentum balance at the core is consistent with the earliest EUC theory and observations (e.g., Fofonoff and Montgomery 1955; Knauss 1960, respectively), inferences from Pacific and Atlantic observations (e.g., McPhaden and Taft 1988; Tang and Weisberg 1993), and direct estimates of the material acceleration in the central Pacific (Qiao and Weisberg 1997). While the vertically integrated momentum balance tends to be linear, the EUC momentum balance is nonlinear. The cor-

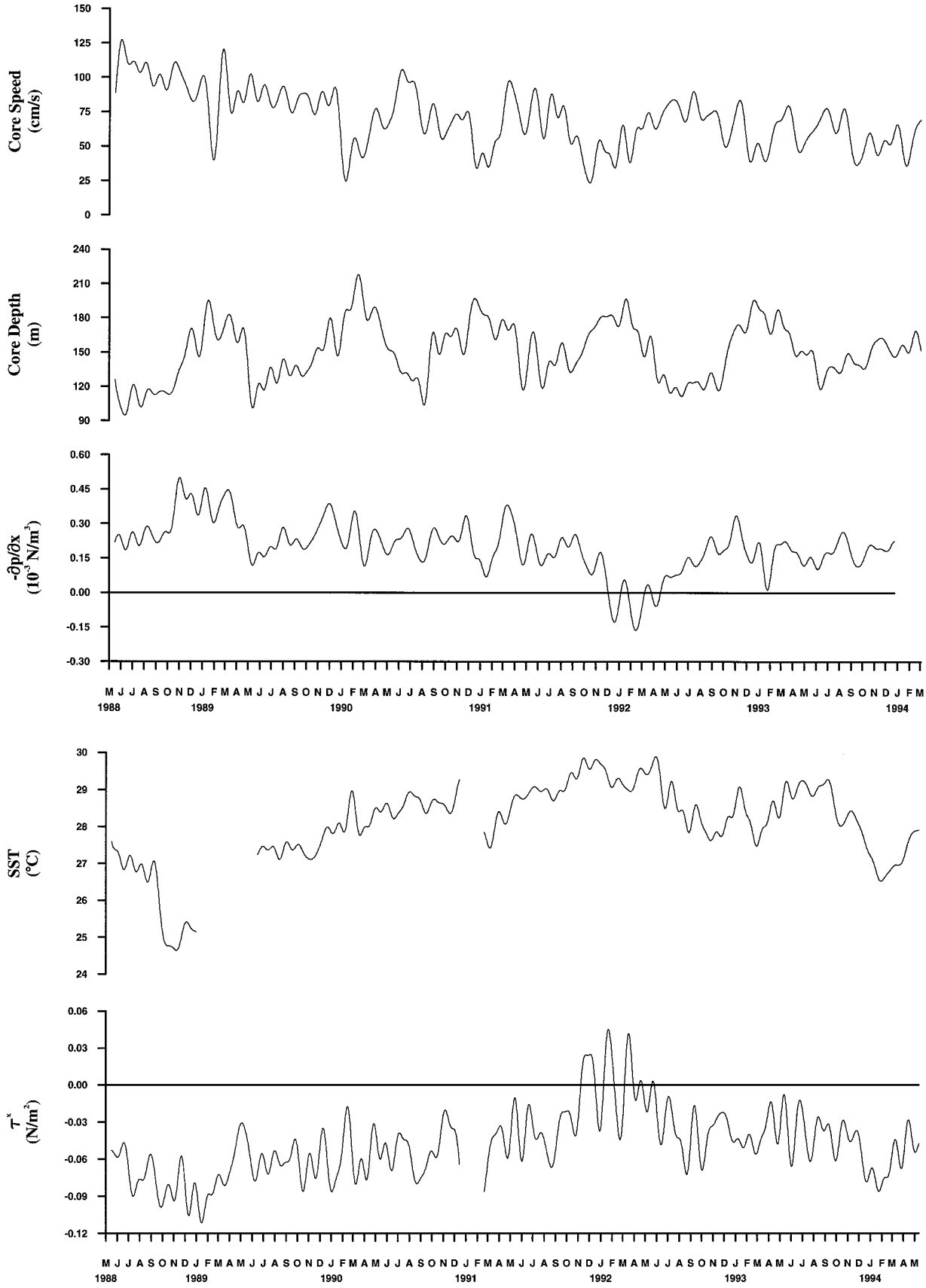
Core Speed (cm/s)
150
125
100
75
50
25
0
Core Depth (m)
240
210
180
150
120
90
-∂p/∂x (10⁻⁵ N/m³)
0.60
0.45
0.30
0.15
0.00
-0.15
-0.30
M J J A S O N D J F M A M J J A S O N D J F M A M J J A S O N D J F M A M J J A S O N D J F M A M J J A S O N D J F M A M J J A S O N D J F M
1988 1989 1990 1991 1992 1993 1994
SST (°C)
30
29
28
27
26
25
24
τˣ (N/m²)
0.06
0.03
0.00
-0.03
-0.06
-0.09
-0.12
M J J A S O N D J F M A M J J A S O N D J F M A M J J A S O N D J F M A M J J A S O N D J F M A M J J A S O N D J F M A M J J A S O N D J F M A M
1988 1989 1990 1991 1992 1993 1994

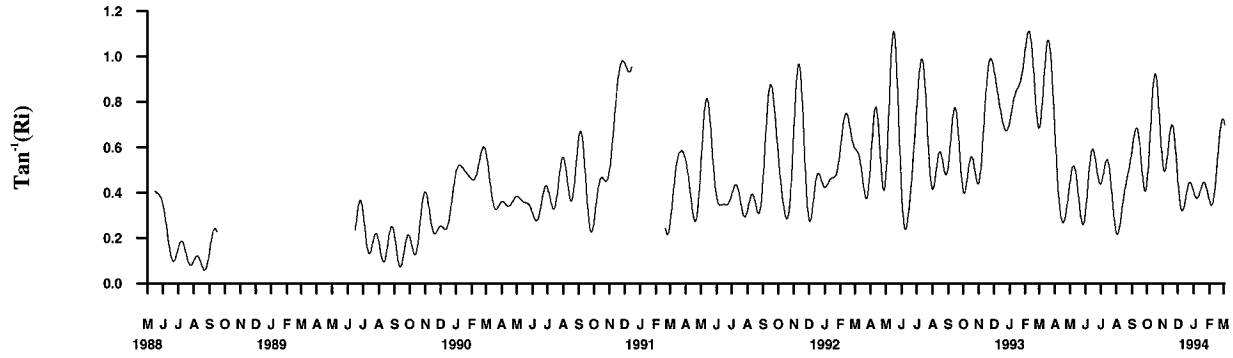

FIG. 3c. Time series of the mixed-layer averaged Tan^{-1} (Ri) at 0°, 170°W low-pass filtered to remove oscillations on timescales shorter than 30 days.

ollary is that the EUC circulation is fully three-dimensional.

c. SST and thermocline

In the eastern equatorial Pacific, interannual variations in SST and thermocline depth are large and correlated, whereas annual variations are not well correlated (e.g., Hayes et al. 1991). This results from annual variability in thermocline depth being small relative to interannual variability, whereas annual variability in SST and wind stress are both large. Thus, the annual cycle in SST is more correlated with the local winds than with the thermocline depth. What is the relationship between SST and thermocline depth in the west-central Pacific and what does this suggest regarding the maintenance of SST on annual and interannual timescales?

A comparison between SST and thermocline depth (Fig. 7) demonstrates that interannual variability exceeds annual variability for SST, whereas interannual, annual, and intraseasonal variations are all prominently observed for thermocline depth. Thus, thermocline depth is not well correlated with SST in the west-central Pacific. For example, the thermocline is deepest in the winters preceding the 1992 El Niño winter and it is shallowest in late winter–spring 1992 while SST is still high. Contrasted with thermocline depth, then, the interannual variations in west-central Pacific SST are correlated with τ^x (Fig. 3b). Specifically, the slow warming in SST from the 1988 La Niña to the 1992 peak El Niño is associated with the slow weakening in τ^x.

The interannual correlation between SST and τ^x may be due to several factors, including the positive feedback between SST and τ^x related to ocean dynamics eluded to earlier. The basis for this feedback is that increasing SST decreases easterly wind stress, which, in turn, further increases SST by decreasing either upwelling or entrainment. We refer to this mechanism of positive feedback later as an SST-zonal wind stress feedback. Interannually, beginning with the 1988 La Niña through the protracted 1991–94 El Niño, the EUC core speed slowly decreases along with a slow increase in core depth. Varying τ^x varies the ZPG and since the ZPG is the driving force for the EUC, there should be a correlation between the ZPG and the EUC core speed. As the fully three-dimensional circulation associated with the EUC and τ^x decreases, it follows that upwelling and entrainment (as evidenced by increasing Ri) decreases, leading to warming. Such warming is envisaged as a fully three-dimensonal consequence of the circulation that, at least locally, is not well correlated with thermocline depth.

d. Horizontal SST advection

Relative to the implied importance of vertical advection and vertical mixing (entrainment) in affecting SST, how important is horizontal advection? The contribution of horizontal advection to the local rate of change of SST ($\partial T/\partial t$) was estimated using the velocity at 170°W and the zonal SST gradient computed from the TAO moorings at 165°E and 140°W. On intraseasonal timescales $\partial T/\partial t$ is found to lead the zonal advection by 1–2 months suggesting that zonal advection cannot cause the local change of SST. Since the zonal SST gradient may be poorly estimated by this large-scale TAO SST difference, the calculation was repeated using the Reynolds' blended SST product (Reynolds and Smith 1995) with similar results for zonal advection, meridional advection, and their sum. These results are shown in Fig. 8. Arranged from top to bottom are SST, the u component averaged over the mixed layer (u_m), the zonal

←

FIG. 3. (a) Time series of u at the EUC core depth, the depth of core, and the ZPG at the core estimated at 0°, 170°W. All time series have been low-pass filtered to remove oscillations on timescales shorter than 30 days. (b) Time series of SST and τ^x at 0°, 170°W low-pass filtered to remove oscillations on timescales shorter than 30 days.

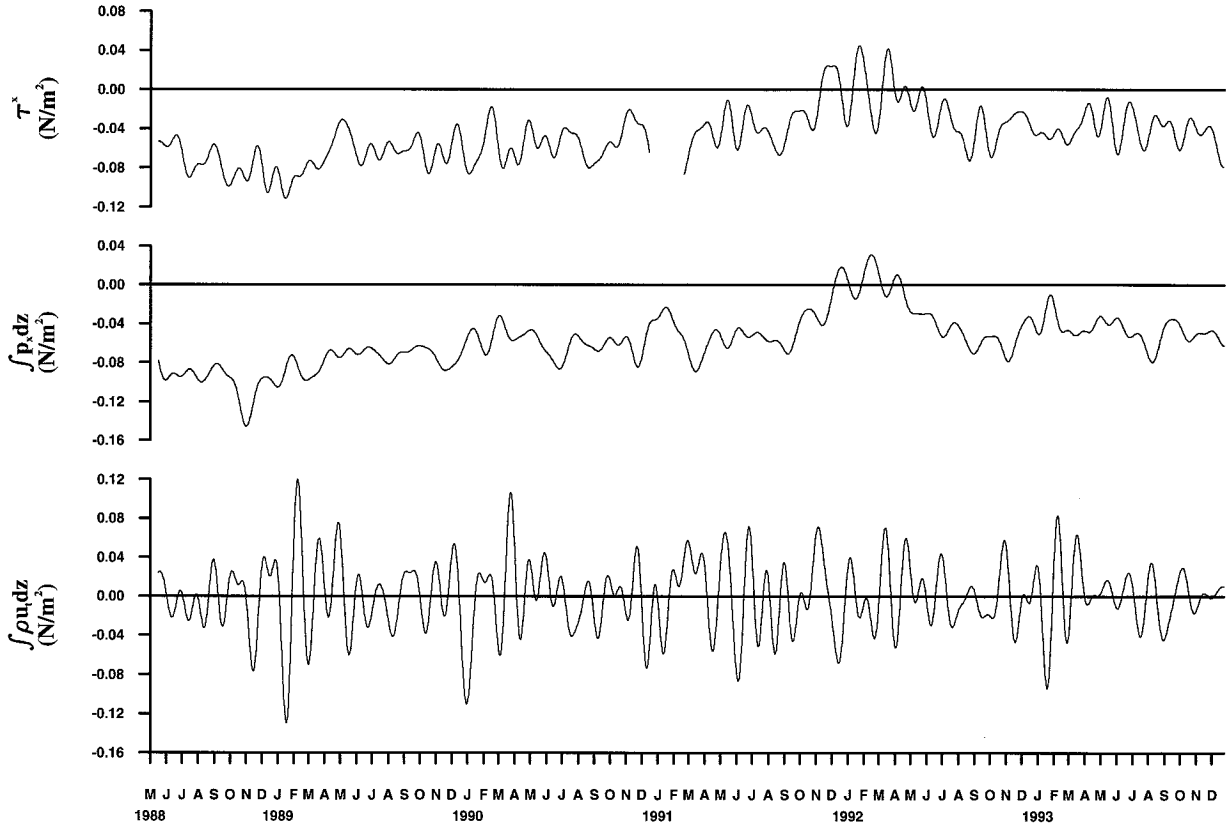

FIG. 4. Time series of τ^x, the vertically integrated ZPG and the vertically integrated local acceleration at 0°, 170°W, low-pass filtered to remove oscillations on timescales shorter than 30 days.

SST gradient, and $\partial T/\partial t$ superimposed upon the zonal advection term; all low-pass filtered to exclude fluctuations on timescales shorter than 30 days and $\partial T/\partial t$ superimposed upon the zonal advection term; low-pass filtered to exclude fluctuations on timescales shorter than 90 days. Several points are noted. First, both u_m and the zonal SST gradient are generally negative, so that zonal advection ($-u_m \partial T/\partial x$) generally acts to cool rather than warm SST. Zonal advection, therefore, does not account for the observed slow warming trend. Second, zonal advection on intraseasonal timescales generally lags $\partial T/\partial t$, indicating that processes other than zonal advection must be important in controlling $\partial T/\partial t$ on intraseasonal timescales. There are times when zonal advection covaries with $\partial T/\partial t$, for example, the fall–winter period of 1992/93, but even then advection has a cooling bias from the observed $\partial T/\partial t$. Third, the November–December 1991 period (during the peak El Niño warming) showed the largest intraseasonal Kelvin wave of the entire record with mixed layer-averaged speed of 80 cm s^{-1}. But, even this largest Kelvin wave pulse had only marginal impact on $\partial T/\partial t$. The more the time series are filtered the easier it is to see the general cooling effect of zonal advection and the phase lag relative to $\partial T/\partial t$ (lower panel). Similar results (not shown) occur upon adding meridional advection. Thus, for both interannual and intraseasonal timescales, west-central Pacific SST appears to be controlled by processes other than horizonal advection.

e. Sensible and latent heat fluxes

Following Hayes et al. (1991), bulk formulas were used to calculate the sensible (Q_{Sen}) and latent (Q_{Lat}) heat fluxes from the TAO array data:

$$Q_{\text{Sen}} = \rho_a C_p C_E U_a (T - T_a), \tag{1}$$

$$Q_{\text{Lat}} = \rho_a L C_E U_a [q_s(T) - RH q_s(T_a)], \tag{2}$$

where T and T_a are the SST and the AT; $\rho_a = 1.225$ kg m^{-3} and $C_P = 1.005 \times 10^3$ J kg^{-1} °C^{-1} are the air density and heat capacity, respectively; $C_E = 1.2 \times 10^{-3}$ is the exchange coefficient; L $= 2.44 \times 10^6$ J kg^{-1} is the latent heat of vaporization; RH is the relative humidity fixed at 0.8; and $U_a = \sqrt{u_a^2 + v_a^2}$ is the surface wind speed. The saturated moisture content q_s is given by the Clausius–Clapeyron equation

$$q_s(T) = q_0 10^{(9.4 - 2353/T)}, \tag{3}$$

where $q_0 = 6.14 \times 10^{-4}$ and T is in kelvins.

The resulting Q_{Sen} and Q_{Lat} are shown as a function of time and longitude along the equator in Fig. 9 and

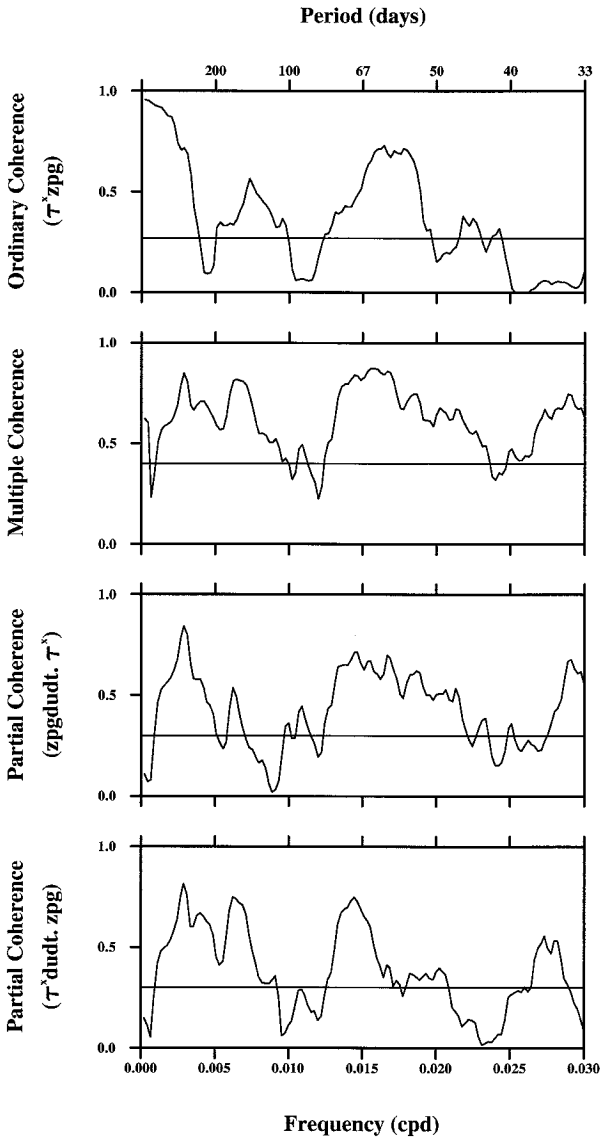

FIG. 5. Coherence analysis between τ^x, the integrated ZPG and the integrated local acceleration. From top to bottom: the ordinary coherence squared between τ^x and the integrated ZPG; the multiple coherence squared between both τ^x and the integrated ZPG with the local acceleration; the partial coherence squared between the integrated ZPG and the local acceleration after removing the influence of τ^x from both of these time series and the partial coherence squared between τ^x and the local acceleration after removing the influence of the integrated ZPG from both of these time series. Averaging was performed over a bandwidth (ΔB) of 0.0036 cpd for approximately 17 degrees of freedom, and the 90% significance levels for the null hypothesis are as shown.

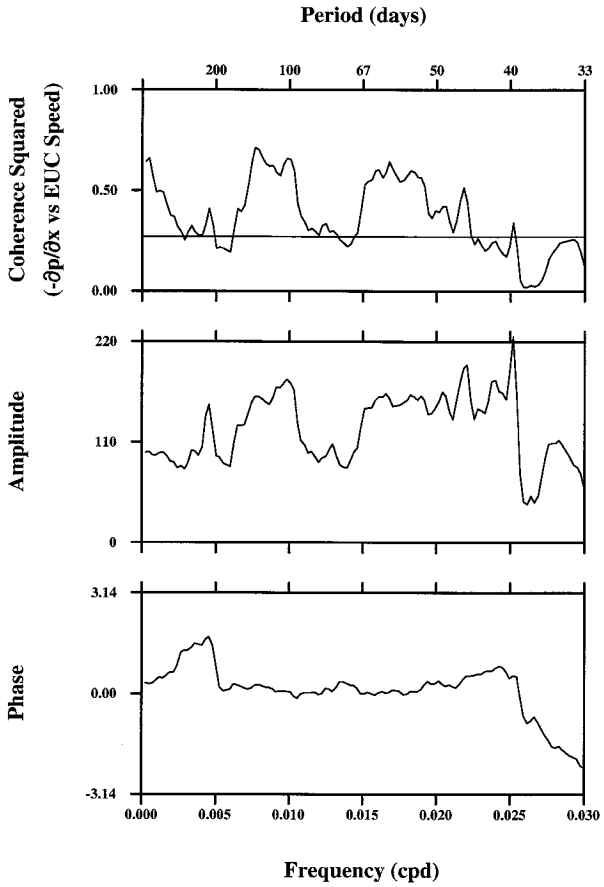

FIG. 6. Coherence analysis between the EUC core speed and the ZPG at the EUC core depth. From top to bottom: the coherence squared, transfer function amplitude, and phase. Averaging was performed over a bandwidth (ΔB) of 0.0036 cpd for approximately 17 degrees of freedom, and the 90% significance level for the null hypothesis is shown for coherence squared.

10, respectively. Slow interannual variations, similar to those of the dynamical variables presented above are observed in these ocean–atmosphere interaction thermodynamical variables. Here, Q_{Sen} tends to have largest positive values in the western Pacific compared with small positive or negative values over the eastern Pacific. Beginning with the 1988 La Niña conditions and culminating with the 1992 peak El Niño warming the region of large, positive Q_{Sen} expands eastward from the western Pacific. Following the peak warming this large, positive Q_{Sen} region then retreats back toward the western Pacific. Here, Q_{Lat} behaves similarly. Its region of largest values, generally found over the western portion of the domain, expands eastward along with the El Niño warming trend. The evolution of this slow, interannual trend in the ocean–atmosphere interaction thermodynamics is most clearly evident in the Bowen ratio (the ratio of Q_{Sen} to Q_{Lat}), as shown in Fig. 11. The Bowen ratio is positive most of the time (positive Q_{Sen}), reflecting the fact that SST exceeds AT. The largest values are found over the western half of the basin and during the transition from La Niña to El Niño the Bowen ratio increases and the region of large values expands eastward into the west-central Pacific. The increase in Bowen ratio shows that while Q_{Lat} greatly exceeds Q_{Sen}, the latter increases proportionately more than the former. Thus, in all of these quantities (including the SST – AT difference) there is a slow, secular rise in magnitude

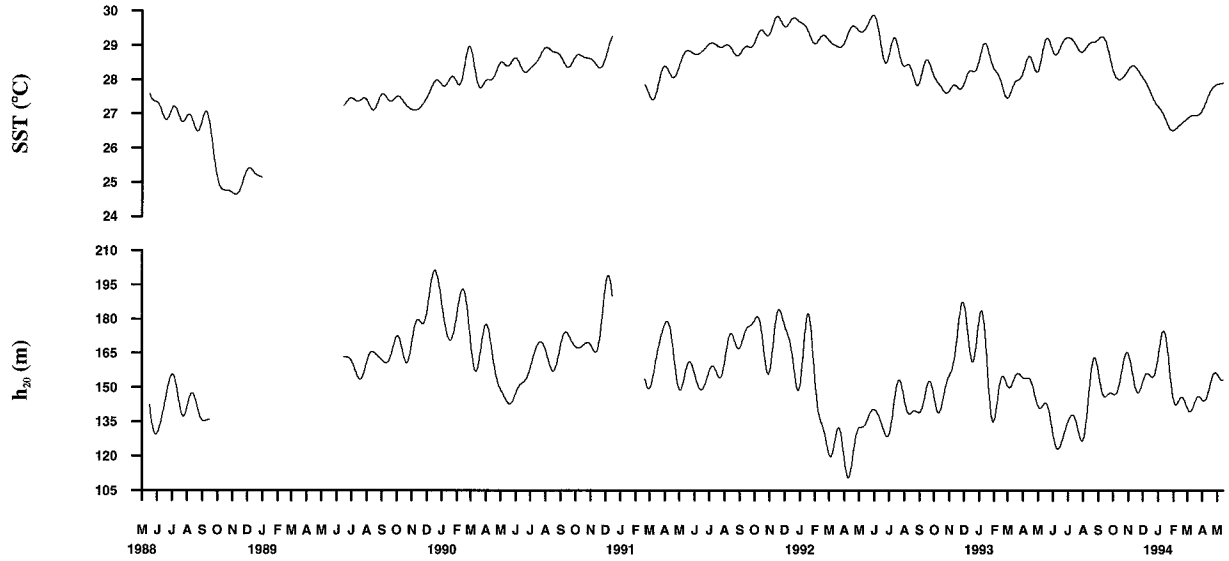

FIG. 7. Time series of SST and the 20°C isotherm depth at 0°, 170°W, low-pass filtered to remove oscillations on timescales shorter than 30 days.

and an eastward expansion in pattern going from the 1988 La Niña to the 1992 peak El Niño, followed by a slow, secular decrease and pattern retreat back toward the western Pacific.

An increase (decrease) in Q_{Sen} and Q_{Lat} effects cooling (warming) upon the ocean. During the warm phase of ENSO, the region of maximum heat loss from the ocean to the atmosphere, which had been located in the west [consistent with the Esbensen and Kushnir (1981) and Oberhuber (1988) climatologies], moves eastward into the central Pacific. The increase in Q_{Sen} and Q_{Lat} over the central (and eastern) Pacific during El Niño requires that the El Niño–warmed ocean remains in contact with relatively cold, dry air. In fact, the largest differences between SST and AT along the equator during the 1988 La Niña to the 1992 peak El Niño transition are found to penetrate eastward into the west-central Pacific (Fig. 12) along with Q_{Sen} and Q_{Lat}. Thus, despite interannual SST variability being maximum over the eastern part of the basin, interannual SST-AT and Q_{Sen} and Q_{Lat} variability are maximum over the west-central part of the basin. The slow-mode behavior in the ocean dynamics is therefore mirrored by slow-mode behavior in the ocean–atmosphere interaction thermodynamics, with the west-central Pacific region of largest interannual τ^x variability coincident with that of Q_{Sen} and Q_{Lat}.

To assess the effects of Q_{Sen} and Q_{Lat} on the coupled ocean–atmosphere system, their origin and their cooling influence, an examination is made into the relationships between the combined heat flux Q (the sum of Q_{Sen} and Q_{Lat}), SST, the wind speed, and the local rate of change of SST with time. Time series of these quantities at 0°, 170°W, low-pass filtered to remove oscillations at timescales shorter than 30 days, are shown in Fig. 13. From the bulk formulas it is known that variations in Q result primarily from variations in T and U_a. These variations in Q, in turn, can affect $\partial T/\partial t$ through the ocean's temperature equation.

A multiple coherence analysis between U_a, T, and Q shows that most of the Q variance occurring at intraseasonal timescales are accounted for by U_a and T as inputs (Fig. 14). A partial coherence analysis (also shown in Fig. 14) determines which of these two variables is most important. Large partial coherence between U_a and Q, after removing the influence of T from both of these time series, shows that U_a is the dominant input variable, since in comparison the partial coherence between T and Q, after removing the influence of U_a from both of these time series, is relatively nil. The Q variations also occur in phase with those of U_a as observed in Fig. 13. This implies that the change in heat flux derived from the bulk formulas is mostly controlled by the change in wind speed, rather than by the change in the SST (at least out to the 10-day cutoff used to filter the data).

Given that Q is determined primarily by U_a, Fig. 15 shows the effect of Q on $\partial T/\partial t$. On intraseasonal timescales, Q and $\partial T/\partial t$ are coherent and π radians out of phase. This is consistent with $\partial T/\partial t$ responding to Q, implying that the local SST change is largely due to the heat flux (recall that advection did not appear to be causal). On interannual timescales, in contrast, $\partial T/\partial t$ does not respond directly to Q. Rather, Q provides a dissipative influence.

In summary, these analyses suggest that on intraseasonal timescales the combined Q_{Sen} and Q_{Lat} varies primarily in response to wind speed, versus SST, and that the rate of change of SST is then determined largely by surface heat flux through the ocean's temperature equation. On interannual timescales, the rate of change of

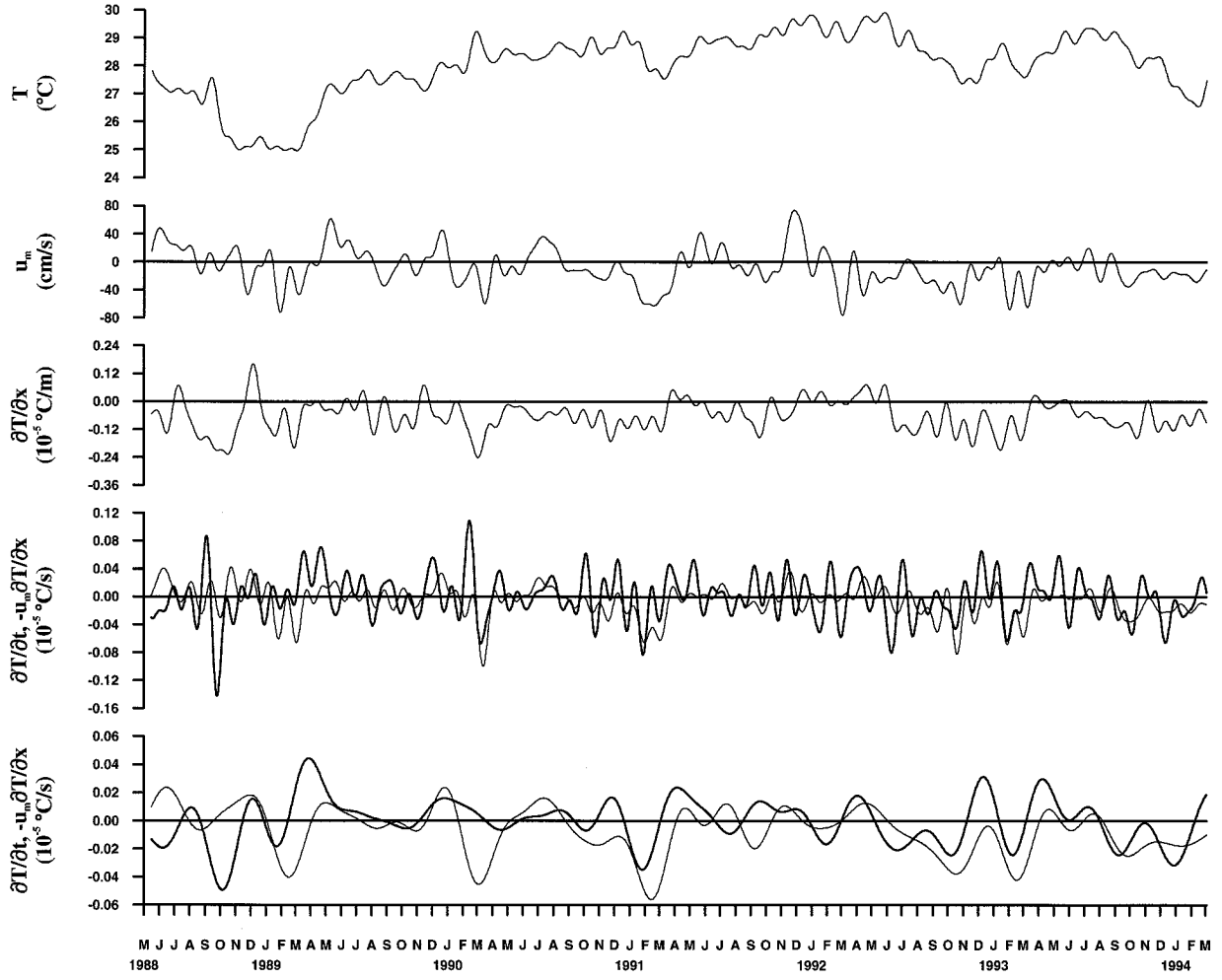

FIG. 8. Time series of the Reynolds' SST, the mixed-layer averaged u_m, the zonal SST gradient and the zonal advection term superimposed upon the local rate of change of the Reynolds' SST (bold line). The data in the top four panels are low-pass filtered to remove oscillations on timescales shorter than 30 days. The data in the bottom panel are low-pass filtered to remove oscillations on timescales shorter than 90 days.

SST must be due to other processes, since the combined Q_{Sen} and Q_{Lat} varies in phase with SST, acting to cool the ocean while SST increases.

These statistical results are supported analytically. For simplicity, with Q_{Lat} greatly exceeding Q_{Sen}, we assume that SST equals AT, allowing Q can be written in terms of the wind speed and the moisture content (proportional to SST via the Clausius Clapeyron equation). Thus, we can write,

$$dQ = (dQ)_{U_a} + (dQ)_{q_s} = \frac{\partial Q}{\partial U_a}\, dU_a + \frac{\partial Q}{\partial q_s}\, dq_s, \quad (4)$$

and then assess the relative importances between the changes in moisture content and wind speed influences via the bulk formulas, whence

$$\frac{(dQ)_{q_s}}{(dQ)_{U_a}} = \frac{2353\ \ln 10 U_a\ dT}{T^2\ dU_a}. \quad (5)$$

When applied to the west-central Pacific using the representative values, $T = 28°\text{C} = 301$ K, $U_a = 5$ m s^{-1}, $dT = 1°$C, and $dU_a = 1$ m s^{-1}, it is found that $(dQ)_{q_s}/(dQ)_{U_a} = 0.3$. This is consistent with the statistical analyses (on intraseasonal timescales) that the surface heat flux is controlled by wind speed. While the ratio between moisture content and wind speed influences increases in the eastern Pacific where T and dU_a are smaller and dT is larger, representative values remain less than unity.

These findings suggest a mechanism of positive SST–wind speed feedback operating through the surface heat flux that can be explained as follows. In response to an increase in SST, the atmosphere shows an increase in cumulus convection and moisture content difference. Convection induces surface wind convergence that lowers wind speed at its center thereby tending to decrease the heat flux. On the other hand, the increase in moisture

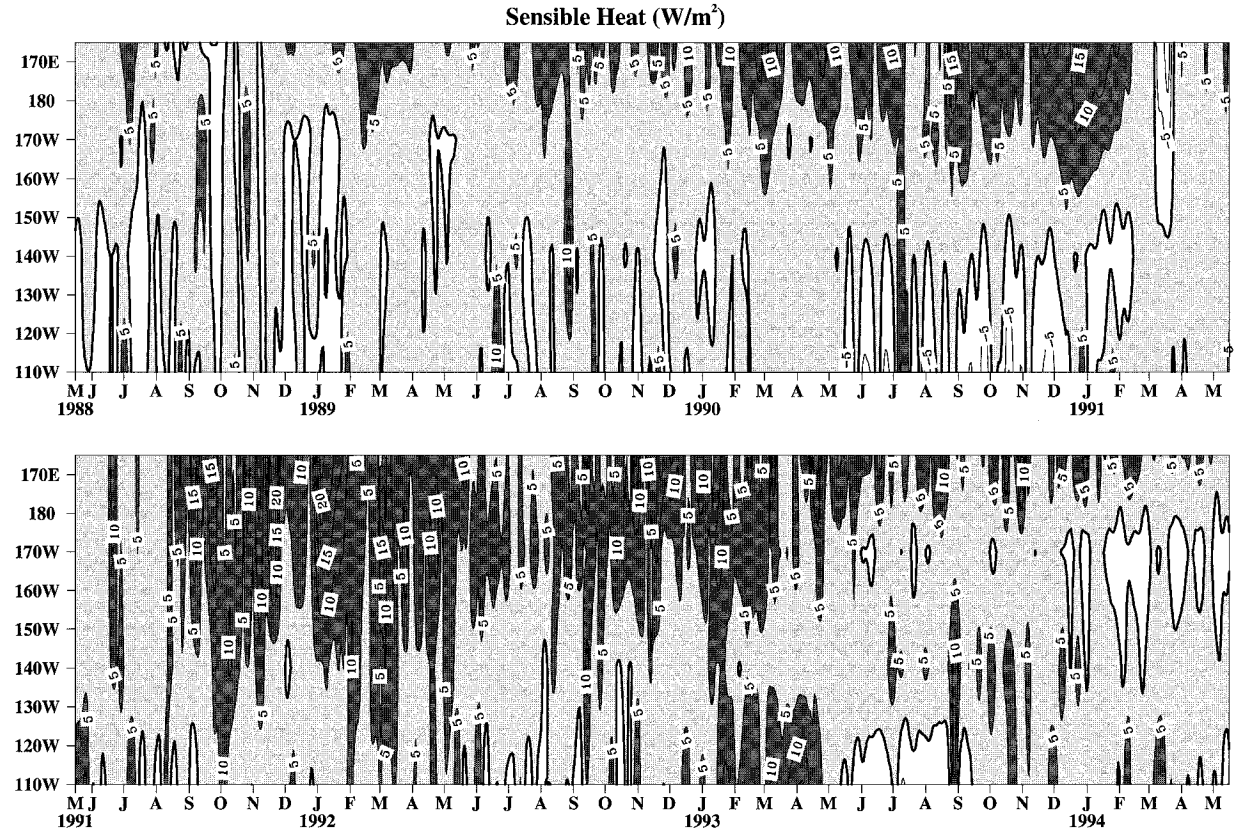

FIG. 9. Sensible heat flux as a function of time and longitude along the equator, calculated from TAO array data, low-pass filtered to remove oscillations on timescales shorter than 10 days. Stippled regions denote positive heat flux with dark stippling in excess of 5 W m^{-2}. Clear regions denote negative heat flux. The contour interval is 5 W m^{-2}.

content difference tends to increase the heat flux. If the heat flux is controlled by wind speed, as shown above for intraseasonal timescales, then the decrease in heat flux due to decreasing wind speed overcomes the increase in heat flux due to increasing moisture content, with the net result being a decrease in heat flux, less ocean cooling, and hence an increase in SST. This positive SST–wind speed feedback, however, may be counteracted by a decrease in solar radiation owing to increased cloudiness. In nature, both the SST–wind speed feedback through surface heat flux and the SST–zonal wind stress feedback through the ocean's dynamical response are likely to be important, offering explanation on why the relationship between SST and thermocline depth is so complicated in the equatorial west-central Pacific.

4. Discussion and summary

Six years of upper-ocean velocity, temperature, and surface meteorological data collected at 0°, 170°W show slow, interannual variability occurring in the dynamics of the ocean circulation and the thermodynamics of ocean–atmosphere interactions. As the transition region between the western Pacific warm pool and the eastern Pacific cold tongue, this west-central Pacific region has large interannual variability in surface wind stress (e.g., Wakata and Sarachik 1991) and it is the region through which both the ocean and atmosphere variabilities associated with ENSO evolve (e.g., Philander et al. 1992). Our analyses focused upon the interannual and intraseasonal aspects of this variability that were found to behave differently.

The measurements began in May 1988, coincident with the La Niña (cold) phase of ENSO, and they have continued through the recent protracted El Niño (warm) phase, which showed peak warming in fall–winter 1991–92. During this time the EUC core speed and τ^x slowly decreased while SST slowly increased. These slow variations are associated with a decrease in the ZPG and an increase in the mixed-layer averaged Ri number. The implication is that the slow SST variability in the equatorial west-central Pacific results from ocean dynamical processes. This may be described as a positive SST–zonal wind stress feedback in which the atmosphere interacts dynamically with the ocean through momentum flux. Decreasing τ^x decreases the ZPG, which decreases the fully three-dimensional upper-ocean circulation. Since it is the ocean circulation that provides for cooling, either through horizontal advec-

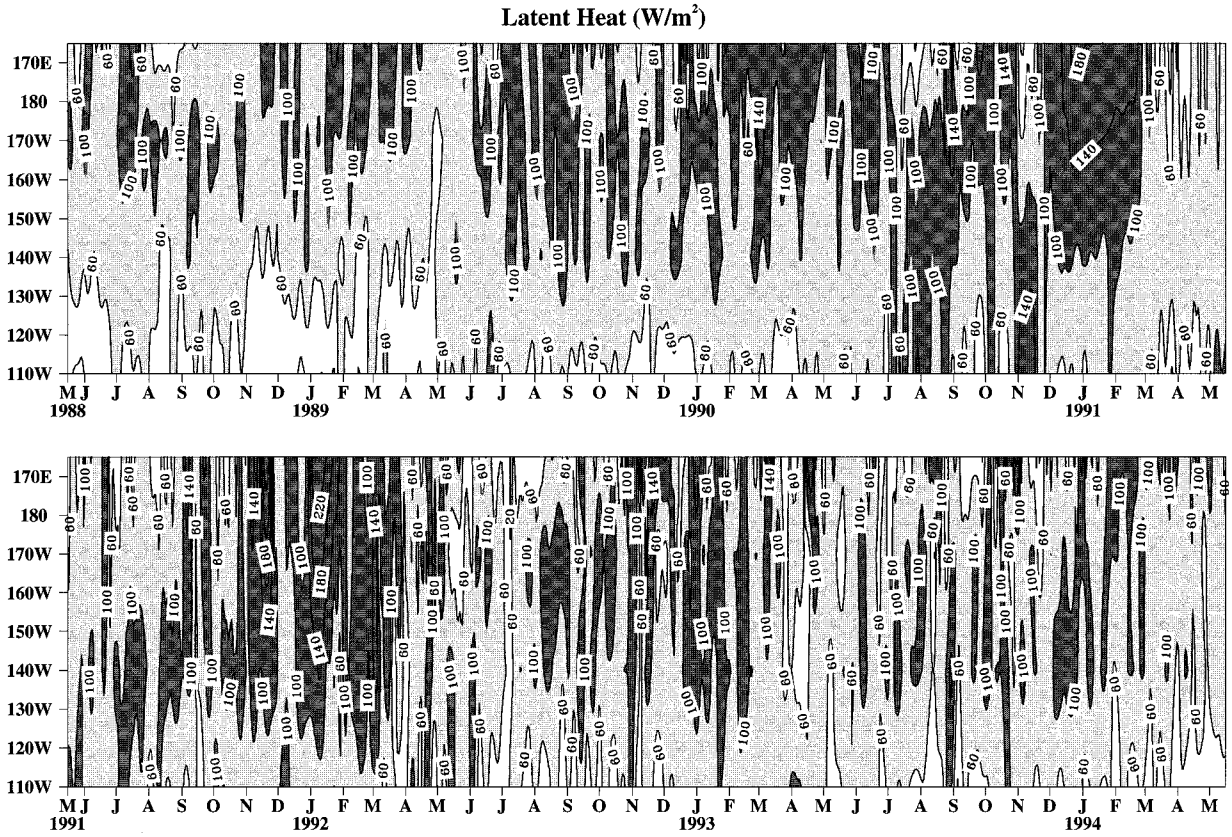

FIG. 10. Latent heat flux as a function of time and longitude along the equator, calculated from TAO array data, low-pass filtered to remove oscillations on timescales shorter than 10 days. Stippled regions denote heat flux larger than 60 W m^{-2} with dark stippling in excess of 100 W m^{-2}. The contour interval is 40 W m^{-2}.

tion, vertical advection (upwelling), or vertical mixing (entrainment), a relaxation of the circulation leads to an increase in SST and, in turn, a further decrease in τ^x. Analyses argue against horizontal advection as a primary factor controlling SST on interannual timescales [contrary to western Pacific warm pool inferences; e.g., McPhaden and Picaut (1990)]. Horizontal advection appears to provide a cooling (rather than a warming) influence in the west-central Pacific. This leaves upwelling and entrainment. Thus, a relaxation of the three-dimensional circulation (as seen in the EUC and implied by the ZPG that drives the EUC) accounts for the slow rise in SST through a deepening of the EUC core and a decrease in entrainment (evidenced in the Ri number). Such reduction in the circulation may occur in two ways: 1) since the EUC normally accelerates (shoals) downstream across the west-central Pacific region an eastward shift of the large-scale system of winds and currents during the La Niña to El Niño transition will result in a decrease (increase) in the EUC core speed (core depth) and 2) a basin-wide decrease in easterly wind stress will also cause the circulation to decrease.

These slow variations observed in the ocean circulation dynamics are mirrored in the ocean–atmosphere interaction thermodynamics. Accompanying the 1988 La Niña to the 1992 peak El Niño transition are secular increases in both Q_{Sen} and Q_{Lat} and the Bowen ratio, with maximum values for these quantities extending eastward into the central Pacific from the west. From the peak warming through the end of the present record (spring 1994), these thermodynamic quantities then show a slow decrease and a pattern retreat back toward the western Pacific.

The dynamical/thermodynamical relationships are different on intraseasonal and interannual timescales. Interannually, τ^x and the vertically integrated ZPG vary in phase, suggesting a slowly varying steady state, while intraseasonally they exhibit a phase lag, necessitating a local acceleration to account for their imbalance. Although analyses show that the local acceleration and ZPG are equally coherent with τ^x on intraseasonal timescales, the coarse TAO array zonal spacing does not resolve the ZPG well enough on intraseasonal timescales to bring closure on the momentum balance. Interannually, SST and the surface fluxes vary in phase (the fluxes cool as SST increases), while intraseasonally they vary in quadrature, consistent with the local rate of change of SST being forced by the net Q_{Lat} and Q_{Sen}. Moreover, horizontal SST advection lags the local rate of change of SST. Thus, neither on interannual nor in-

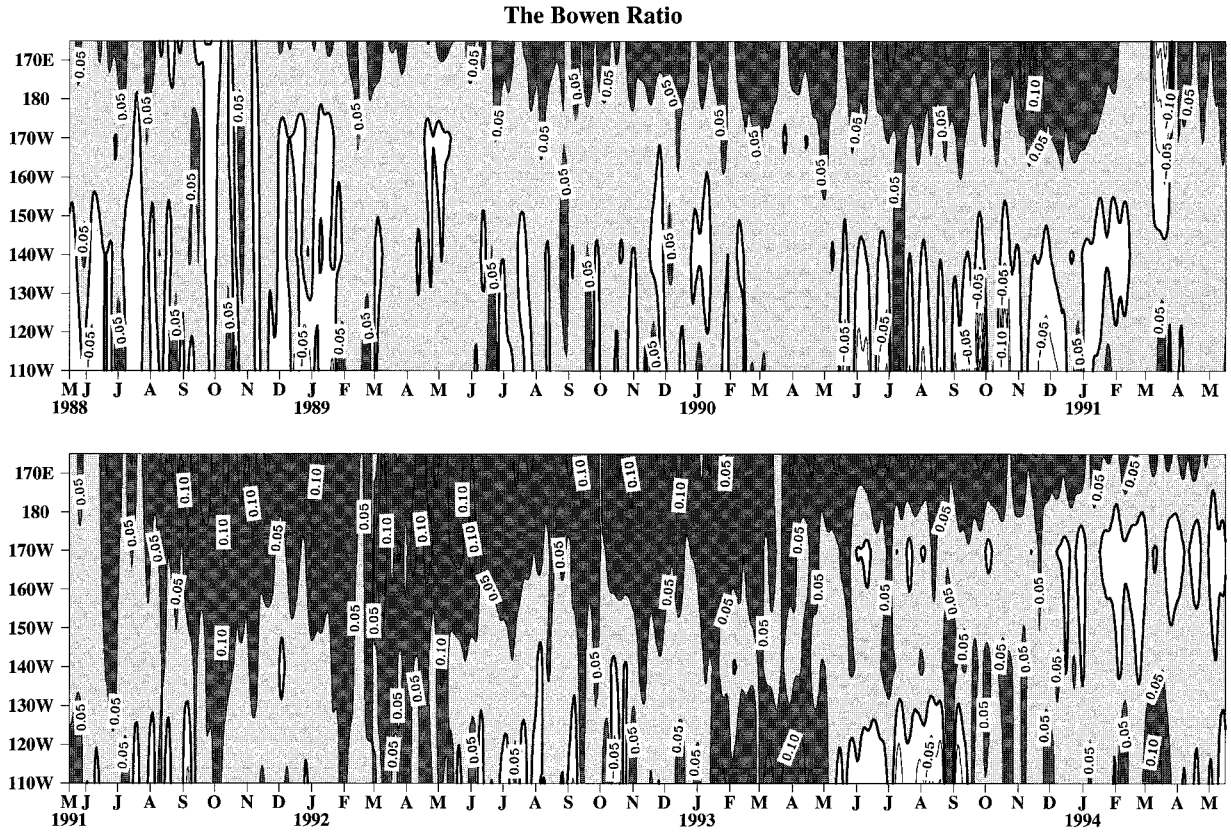

FIG. 11. The Bowen ratio as a function of time and longitude along the equator, low-pass filtered to remove oscillations on timescales shorter than 10 days. Stippled regions denote positive values with dark stippling in excess of 0.05; clear regions denote negative values and the contour interval is 0.05.

traseasonal timescales does horizontal advection appear to be a causal factor for local SST variability at 0°, 170°W.

The relative importances of SST and wind speed in the bulk-formulas-derived surface heat flux was analyzed for intraseasonal timescales [related analyses for subsets of data over the period 1991–93 are presented by Zhang and McPhaden (1995)]. Wind speed is found to be the dominant factor and this is supported analytically for Q_{Lat} (which greatly exceeds Q_{Sen}). The local rate of change of SST is therefore proportional to wind speed, with increasing wind speed tending to reduce SST. This SST–wind speed feedback through surface heat flux differs from the SST–zonal wind stress feedback through momentum flux and it may complicate El Niño evolution. For example, fall–winter 1989–90 provides a sequence of events that look like a developing El Niño, yet nothing happened. The Southern Oscillation index was dropping, SST was warming, reaching a peak at the end of February 1990 following a burst in westerly winds, but conditions shortly thereafter returned to normal. The wind speed, however, was high, which, through the SST–wind speed feedback, would tend to decrease SST rather than increase it. In contrast, the westerly wind bursts in fall–winter 1991–92 had lower speeds in the west-central Pacific.

With SST controlled by different processes on interannual and intraseasonal timescales, it is not surprising that SST variability in the west-central equatorial Pacific is not well correlated with thermocline depth. This differs from the eastern Pacific where the thermocline is shallow and SST and thermocline depth are correlated on interannual timescales. Such regional dependence of SST on thermocline depth is consistent with different controlling processes (e.g., Chang 1993; Koberle and Philander 1994). Here we have suggested two influences, one operating interannually through momentum flux and the other operating intraseasonally through heat flux.

The momentum flux argument for slowly increasing SST in response to slow, synchronous decreases in τ^x and ZPG is that the ocean dynamics (through upwelling and entrainment) provides a cooling influence upon SST. Relaxing this ocean dynamical effect therefore leads to warming. The cooling is tied to the three-dimensional circulation of the EUC. Decreasing the circulation decreases upwelling and entrainment, and without a concomittant decrease in net radiation this would lead to

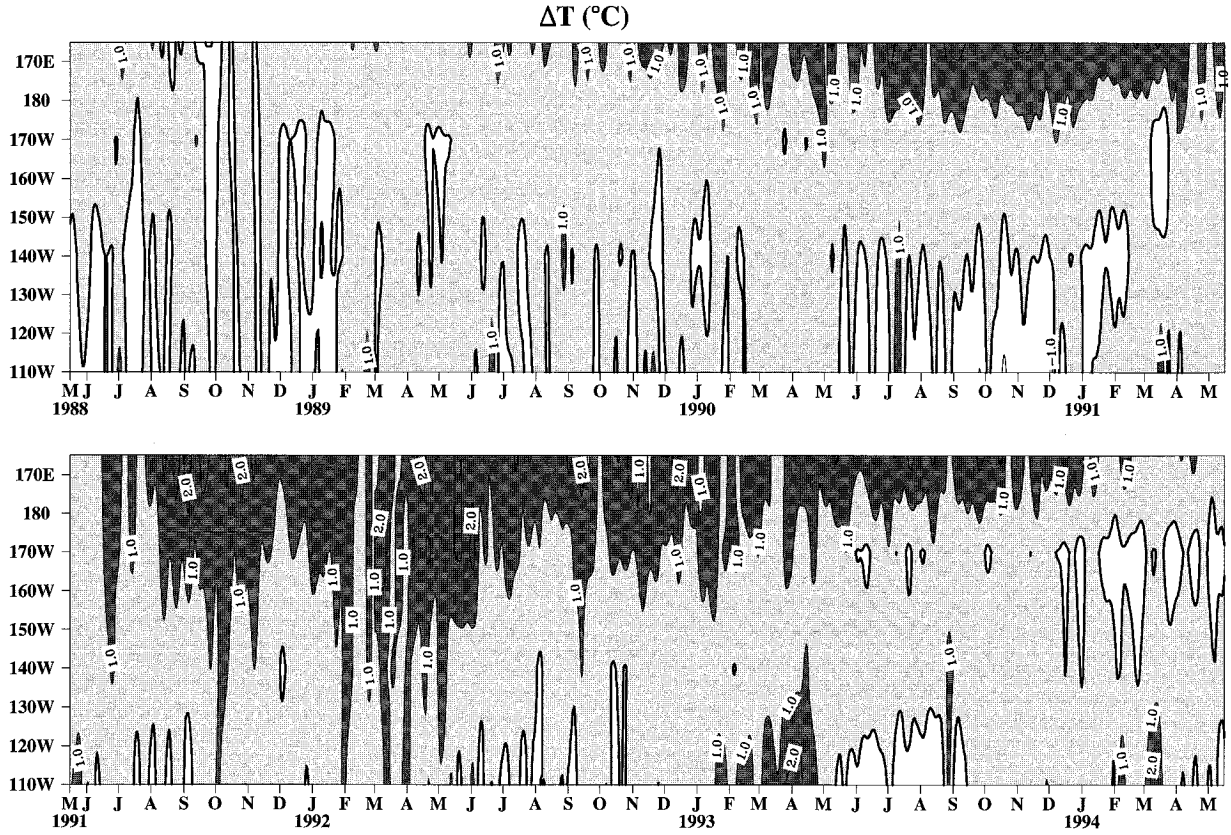

FIG. 12. SST – AT difference as a function of time and longitude along the equator, calculated from the TAO array data, low-pass filtered to remove oscillations on timescales shorter than 10 days. Stippled regions denote positive values with dark stippling in excess of 1°C; clear regions denote negative values and the contour interval is 1°C.

warming. As SST warms, Q_{lat} and Q_{Sen} tend to cool, providing a dissipative effect. The synchronous, interannual variations observed in τ^x, ZPG, EUC core depth and speed, SST, Q_{lat}, and Q_{Sen} may therefore be described as a slow mode, with the oceans contribution being a fully three-dimensional divergence mode related to the EUC.

The atmosphere's contribution also appears to be a fully three-dimensional divergence mode. This may be deduced from the Q_{lat} and Q_{Sen} distributions. As these heat fluxes increase with increasing SST and decreasing τ^x (and wind speed), the Bowen ratio also increases. This means that the affect of the SST – AT difference outweighs the nonlinear affect of the Clausius Clapeyron equation. While Q_{lat} greatly exceeds Q_{Sen}, the overlying atmosphere (despite increasing SST) remains relatively cold and dry. Since the ocean's influence on the atmosphere is warming and moistening, the only way that the atmosphere can remain cold and dry is for air to descend from aloft. We thus deduce a counterpart three-dimensional atmosphere divergence mode.

The slow, interannual variations described above may be summarized as a positive feedback mode. What provides the negative feedback required for the coupled ocean–atmosphere system to oscillate and is this different from the delayed oscillator paradigm? We argue below for an origin of negative feedback residing in the western Pacific, drawing upon evidence from two sources: 1) the fact that the Q_{Sen}, Q_{lat}, and Bowen ratio distributions presented herein have maximum values expanding eastward into the central Pacific from the west, while always exhibiting minimum values in the eastern Pacific; 2) correlation patterns between interannual anomaly fields of SST, sea level pressure (SLP), and surface winds presented by Weisberg and Wang (1997).

The first demonstrates that the region of maximum anomalous ocean to atmosphere heat flux during the 1988 La Niña to the 1992 peak El Niño transition was in the west-central Pacific, not the eastern Pacific. This finding is supported by the analyses of Deser and Wallace (1990) and Zebiak (1990), wherein the west-central Pacific is observed or inferred, respectively, as the region of maximum condensation heating. It follows that the west central Pacific is the region of maximum ocean–atmosphere coupling for both momentum and heat flux.

The second shows distinctively different patterns east and west of the dateline for the correlation field between SST and SLP. East of the date line is a broad region of negative correlation, centered on and symmetric about

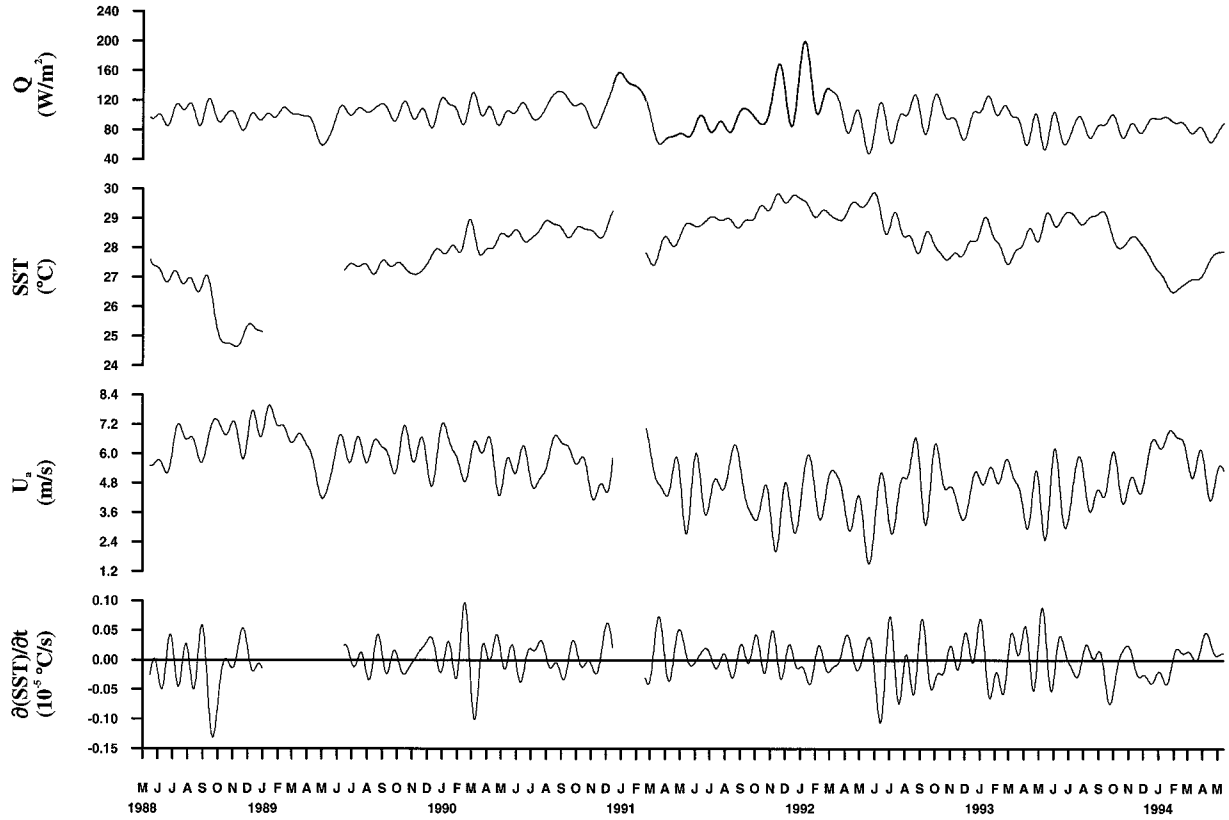

FIG. 13. Time series of the combined (Q_{Sen} plus Q_{lat}) heat flux Q, SST, wind speed, and the local rate of change of SST, calculated from the TAO array data at 0°, 170°W low-pass filtered to remove oscillations on timescales shorter than 30 days. Note that the bold lines in Q represent interpolated values using other TAO array data.

the equator. West of the date line patterns of symmetric, negative correlation are also observed, but located 10°–20° poleward and separated by a region of positive correlation on the equator. These patterns may be explained beginning with a Gill (1980) atmosphere model forced by condensation heating in the west-central equatorial Pacific. The response (Gill 1980) shows a region of low pressure extending eastward and symmetric about the equator in the form of an atmospheric Kelvin wave and a symmetric pair of low pressure, off-equator cyclones located just west of the localized heating in the form of an atmospheric Rossby wave. The Kelvin wave portion of the response accounts for the negative SST–SLP correlation pattern observed in the east. The positive wind stress curl of the off-equator cyclone pair raises the ocean thermocline by Ekman pumping and cools SST, thereby accounting for the off-equator negative SST–SLP correlation pattern observed in the west. Such Ekman pumping and pattern expansion westward as a forced oceanic Rossby wave has been reported by White et al. (1989) and Kessler (1990).

The western Pacific off-equator SST–SLP correlation pattern development, the fact that SLP lags SST by about 1–3 months, the subtlety of the heat flux anomaly necessary to achieve such a pattern, and its relationship to the wind anomalies are described by D. Mayer and R. Weisberg (1997, unpublished manuscript). During the mature phase of El Niño the relatively high off-equator SLP resulting from the relatively low off-equator SST initiates easterly winds over the far western Pacific as observed toward the end of all El Niño warm phases (e.g., Tang and Weisberg 1984; Deser and Wallace 1990; Zebiak 1990; Chao and Philander 1993). These easterlies cause upwelling that progresses eastward as a forced oceanic Kelvin wave tending to reverse the sign of the SST anomaly over the central Pacific (NINO3 index) region and hence the sign of all related variables.

As conceived above, the western Pacific is hypothesized as being the causal region for ENSO. Positive SST–zonal wind stress feedback causes the region of maximum condensation heating to migrate eastward into the west-central Pacific until it is sufficiently far east to allow for an off-equator negative SST–SLP correlation to develop in the west. This reverses the sign of the equatorial SST anomaly in the central Pacific causing the region of maximum convection to retreat back to the west. The connections are illustrated in Fig. 16. Condensation heating in the west-central Pacific results in off-equator cyclones. These cause off-equator cold SST anomalies in the western Pacific by Ekman pumping resulting in off-equator high SLP anomalies. These

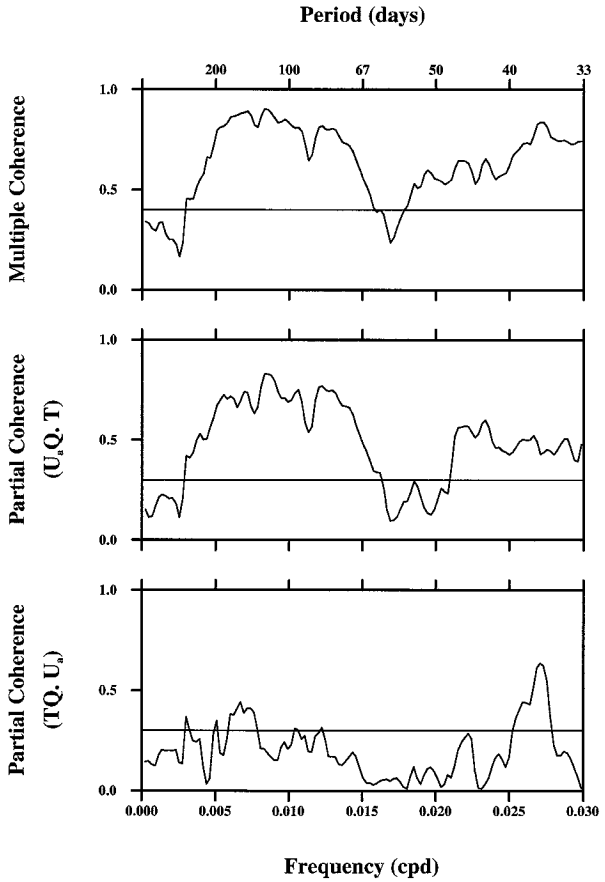

FIG. 14. Multiple coherence analysis between SST and the wind speed with the heat flux. From top to bottom: the multiple coherence squared between SST and the wind speed with the heat flux, the partial coherence squared between the wind speed and the heat flux after removing the influence of SST from both of these, and the partial coherence squared between SST and the heat flux after removing the influence of the wind speed from both of these. Averaging was performed over a bandwidth (ΔB) of 0.0036 cpd for approximately 17 degrees of freedom and the 90% significance levels for the null hypothesis are as shown.

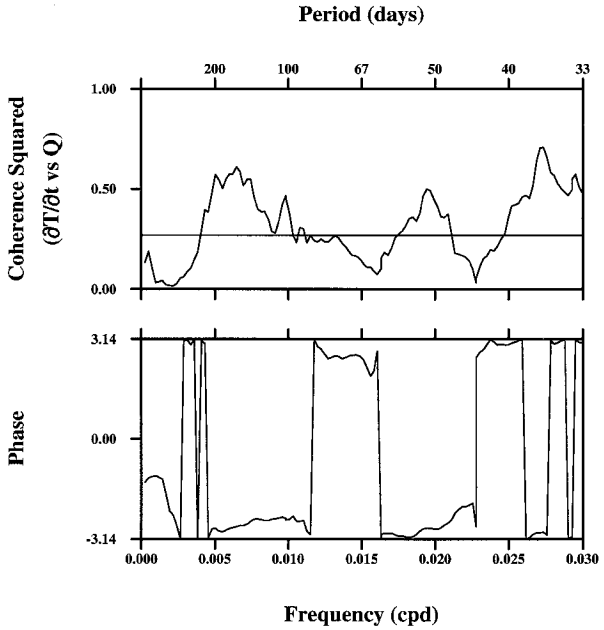

FIG. 15. Coherence squared and phase between the local rate of change of SST and the combined heat flux. Averaging was performed over a bandwidth (ΔB) of 0.0036 cpd for approximately 17 degrees of freedom and the 90% significance level for the null hypothesis on coherence squared is shown.

off-equator high SLP anomalies then initiate easterly winds over the far western equatorial Pacific providing a negative feedback to reverse the sign of the equatorial central Pacific SST anomalies.

In summary, 6 yr of observations in the west-central Pacific, as part of the TAO array, show slow, synchronous variations in the upper-ocean circulation, winds, SST, and surface fluxes during the transition from the 1988 La Niña to the 1992 peak El Niño. These observations suggest a coupled slow-mode operating within the ocean–atmosphere system having oceanic and atmospheric elements that are fully three-dimensional divergence modes. The oceanic portion is deduced as related to the overturning circulation of the EUC and the atmospheric portion is deduced as related to the Walker Circulation. As conceived, these ocean and atmosphere modes differ from previous slow modes within reduced-gravity models (e.g., Hirst 1988; Neelin 1991; Wang and Weisberg 1994) in that 1) the internal workings of the layers, as opposed to just their vertical integrals, are important in determining SST and the overlying AT and moisture content and 2) the symmetry properties are different over the eastern and western sides of the basin. They also differ from the delayed oscillator paradigm (e.g., Schopf and Suarez 1988; Battisti and Hirst 1989; Cane et al. 1990; Chao and Philander 1993) in that 1) negative feedback is provided by coupled ocean–atmosphere waves originating over the western part of the basin, as contrasted with free ocean waves reflecting at the western boundary and 2) the west-central Pacific, as contrasted with the eastern Pacific, is the region of maximum anomalous ocean–atmosphere coupling for both heat and momentum. Our hypothesis, thus deduced, may be described as a hybrid mode between these existing ENSO paradigms and it may work in a complementary manner with the delayed oscillator mechanism.

Acknowledgments. The U.S. Department of Commerce, National Oceanic and Atmospheric Administration, Office of Global Programs provided support for field work and initial analyses under Grant Numbers NA87AA-D-AC120 and NA36GP01431 and for continued analyses under Grant Number NA66GP0119. The University of South Florida, Division of Sponsored Research, provided equipment matching and assisted with support when field work funding ended. We are particularly indebted to (the late) Dr. Stanley B. Hayes

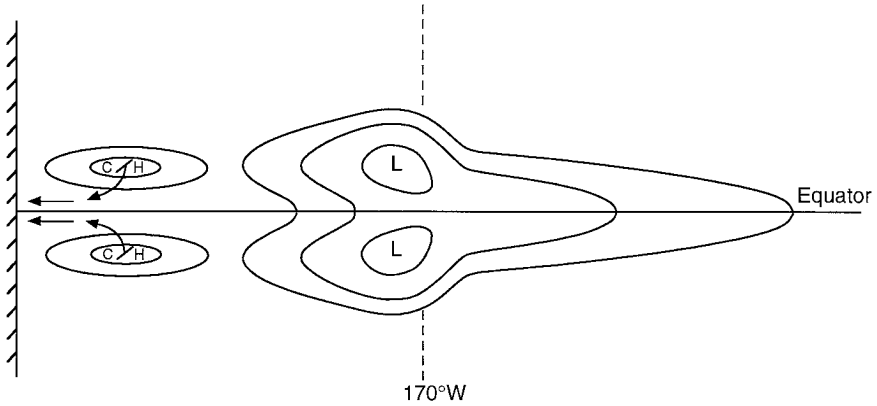

FIG. 16. A schematic diagram of the connections, providing a negative feedback during the mature phase of ENSO, between condensation heating in the west-central Pacific and easterly winds over the western Pacific. Condensation heating (as adapted from Gill 1980) results in an off-equator cyclone pair. This causes a pattern of off-equator cold SST/high SLP correlation by Ekman pumping and air–sea interaction. Off-equator high SLP then drives equator-convergent easterly winds over the western Pacific. These easterly winds force upwelling that propagates eastward, tending to reverse the sign of the SST anomalies in the equatorial central Pacific.

for his assistance in initiating and maintaining the 0°, 170°W site as part of the TOGA TAO array. Dr. Hayes believed very strongly in the importance of academic scientist involvement in all aspects of the TAO array. We are also indebted to Dr. T. Y. David Tang of the National Taiwan University and to the National Science Council, ROC, for assisting with data acquisitions in 1993 during a support hiatus. Dr. Tang and Mr. Dennis Mayer of NOAA/AOML provided many insightful discussions. We also thank the TAO Project Office at NOAA/PMEL for making the TAO array data available.

REFERENCES

Battisti, D. S., and A. C. Hirst, 1989: Interannual variability in a tropical atmosphere–ocean model: Influence of the basic state, ocean geometry and nonlinearity. *J. Atmos. Sci.,* **46,** 1687–1712.

Cane, M. A., M. Munnich, and S. E. Zebiak, 1990: A study of self-excited oscillations of the tropical ocean–atmosphere system. Part I: Linear analysis. *J. Atmos. Sci.,* **47,** 1562–1577.

Chang, P., 1993: Seasonal cycle of sea surface temperature and mixed layer heat budget in the tropical Pacific Ocean. *Geophys. Res. Lett.,* **20,** 2079–2082.

Chao, Y., and S. G. H. Philander, 1993: On the structure of the Southern Oscillation. *J. Climate,* **6,** 450–469.

Deser, C., and J. M. Wallace, 1990: Large-scale atmospheric circulation features of warm and cold episodes in the tropical Pacific. *J. Climate,* **3,** 1254–1281.

Diaz, H. F., and V. Markgraf, 1992: *El Niño: Historical and Paleoclimatic Aspects of the Southern Oscillation.* Cambridge University Press, 476 pp.

Esbensen, S. K., and V. Kushnir, 1981: The heat budget of the global ocean: An atlas based on estimates from surface marine observations. Climate Research Institute Rep. 29, Oregon State University, Corvallis, OR, 27 pp. and 188 figures.

Fofonoff, N. P., and R. B. Montgomery, 1955: The equatorial undercurrent in the light of the vorticity equation. *Tellus,* **7,** 518–521.

Gill, A. E., 1980: Some simple solutions for heat-induced tropical circulation. *Quart. J. Roy. Meteor. Soc.,* **106,** 447–462.

Hayes, S. P., P. Chang, and M. McPhaden, 1991: Variability of the sea surface temperature in the eastern equatorial Pacific during 1986–1988. *J. Geophys. Res.,* **96,** 10 553–10 566.

Hirst, A. C., 1986: Unstable and damped equatorial modes in simple coupled ocean–atmosphere models. *J. Atmos. Sci.,* **43,** 606–630.

——, 1988: Slow instabilities in tropical ocean basin-global atmosphere models. *J. Atmos. Sci.,* **45,** 830–852.

Hisard, P., J. Merle, and B. Voituriez, 1970: The equatorial undercurrent at 170°E in March and April 1967. *J. Mar. Res.,* **28,** 281–303.

Kessler, W. S., 1990: Observations of long Rossby waves in the northern tropical Pacific. *J. Geophys. Res.,* **95,** 5183–5219.

——, and M. J. McPhaden, 1995: The 1991–1993 El Niño in the central Pacific. *Deep-Sea Res.,* **42,** 295–333.

Knauss, J. A., 1960: Measurements of the Cromwell Current. *Deep-Sea Res.,* **6,** 265–286.

Knox, R. A., and D. Halpern, 1982: Long range Kelvin wave propagation of transport variations in Pacific Ocean equatorial current. *J. Mar. Res.,* **40,** 329–339.

Koberle, C., and S. G. Philander, 1994: On the processes that control seasonal variations of sea surface temperature in the tropical Pacific Ocean. *Tellus,* **46A,** 481–496.

Lien, R. C., D. R. Caldwell, M. C. Gregg, and J. N. Moum, 1995: Turbulence variability at the equator in the central Pacific at the beginning of the 1991–1993 El Niño. *J. Geophys. Res.,* **100,** 6881–6898.

McPhaden, M. J., and B. A. Taft, 1988: Dynamics of seasonal and intraseasonal variability in the eastern equatorial Pacific. *J. Phys. Oceanogr.,* **18,** 1713–1732.

——, and J. Picaut, 1990: El Niño–Southern Oscillation displacements of the western equatorial Pacific warm pool. *Science,* **250,** 1385–1388.

——, S. P. Hayes, L. J. Mangum, and J. M. Toole, 1990: Variability in the western equatorial Pacific Ocean during the 1986–87 El Niño/Southern Oscillation event. *J. Phys. Oceanogr.,* **20,** 190–208.

Neelin, J. D., 1991: The slow sea surface temperature mode and the fast-wave limit: Analytic theory for tropical interannual oscillations and experiments in a hybrid coupled models. *J. Atmos. Sci.,* **48,** 584–606.

——, M. Latif, and F.-F. Jin, 1994: Dynamics of coupled ocean–atmosphere models: The tropical problem. *Annu. Rev. Fluid Mech.,* **26,** 617–659.

Oberhuber, J. M., 1988: An atlas based on the 'COADS' data set: The budgets of heat, buoyancy and turbulent kinetic energy at

the surface of the global ocean. Max-Planck-Institut für Meteorologie Rep. 15, Max-Planck-Institut für Meteorologie, Hamburg, Germany, 199 pp.

Peters, H., M. C. Gregg, and J. M. Toole, 1988: On the parameterization of equatorial turbulence. *J. Geophys. Res.*, **93,** 1199–1218.

Philander, S. G., 1990: *El Niño, La Niña, and the Southern Oscillation.* Academic Press, 289 pp.

——, R. C. Pacanowski, N. C. Lau, and M. J. Nath, 1992: Simulation of the ENSO with a global atmospheric GCM coupled to a high-resolution, tropical Pacific Ocean GCM. *J. Climate,* **5,** 308–329.

Qiao, L., and R. H. Weisberg, 1997: The zonal momentum balance of the Equatorial Undercurrent in the central Pacific. *J. Phys. Oceanogr.*, **27,** 1094–1119.

Reynolds, R. W., and T. M. Smith, 1995: A high-resolution global sea surface temperature climatology. *J. Climate,* **8,** 1571–1583.

Suarez, M. J., and P. S. Schopf, 1988: A delayed action oscillator for ENSO. *J. Atmos. Sci.*, **45,** 3283–3287.

Tang, T. Y., and R. H. Weisberg, 1984: On the equatorial Pacific response to the 1982/1983 El Niño–Southern Oscillation event. *J. Mar. Res.*, **42,** 809–829.

——, and ——, 1993: Seasonal variations in equatorial Atlantic Ocean zonal volume transport at 28°W. *J. Geophys. Res.,* **98,** 10 145–10 153.

Wakata, Y., and E. S. Sarachik, 1991: Unstable coupled atmosphere–ocean basin modes in the presence of a spatially varying basic state. *J. Atmos. Sci.,* **48,** 2060–2077.

Wang, C., and R. H. Weisberg, 1994: On the ''slow mode'' mechanism in ENSO related coupled ocean–atmosphere models. *J. Climate,* **7,** 1657–1667.

Weisberg, R. H., and S. P. Hayes, 1995: Upper ocean variability on the equator in the Pacific at 170°W. *J. Geophys. Res.,* **100,** 20 485–20 498.

——, and C. Wang, 1997: A western Pacific oscillator paradigm for the El Niño–Southern Oscillation. *Geophys. Res. Lett,* in press.

White, W. B., Y. H. He, and S. E. Pazan, 1989: Redistribution of subsurface thermal structure during the onset of the 1982–83 and 1986–87 ENSO events and the 1984–85 anti-ENSO event. *J. Phys. Oceanogr.*, **19,** 1397–1406.

Zebiak, S. E., 1990: Diagnostic studies of Pacific surface winds. *J. Climate,* **3,** 1016–1031.

Zhang, G. J., and M. J. McPhaden, 1995: The relationship between sea surface temperature and latent heat flux in the equatorial Pacific. *J. Climate,* **8,** 589–605.